Can an Intermediate Rate of Nitrogen Inversion Affect Drug Efficacy?

Raphael R. Steimbach [1,2], Gergely Tihanyi [1,2], Magalie N. E. Géraldy [1,3], Alicja Wzorek [4], Aubry K. Miller [1,5] and Karel D. Klika [1,*]

[1] Cancer Drug Development, German Cancer Research Center (DKFZ), Im Neuenheimer Feld 280, D-69120 Heidelberg, Germany; r.steimbach@dkfz.de (R.R.S.); gergely.tihanyi@fmi.ch (G.T.); geraldy.mag@hotmail.fr (M.N.E.G.); aubry.miller@dkfz.de (A.K.M.)
[2] Biosciences Faculty, University of Heidelberg, D-69120 Heidelberg, Germany
[3] Bayer AG, Friedrich-Ebert Straße 217/333, D-42117 Wuppertal, Germany
[4] Institute of Chemistry, Jan Kochanowski University in Kielce, Uniwersytecka 7, 25-406 Kielce, Poland; alicja.wzorek@ujk.edu.pl
[5] German Cancer Consortium (DKTK), D-69120 Heidelberg, Germany
* Correspondence: k.klika@dkfz.de; Tel.: +49-6221-42-4515

Supplementary Materials

Abstract

Nitrogen-inversion rates and diffusion coefficients were measured using ^{1}H NMR for 14 drug-like molecules. The slow nitrogen-inversion rates of these molecules lay within a postulated intermediate range in terms of their ability to bind to proteins bounded by diffusion constraints, potentially affecting the availability, hence efficacy, of these compounds if they were utilized as drugs. The postulated intermediate range is based on a capture-volume concept, whereby the nitrogen inversion during the time a ligand takes to pass through a volume surrounding the protein binding site, as calculated by the diffusion rate, determines if it will influence ligand binding to the protein. In the systems examined here, the measured nitrogen-inversion rates and the times required to traverse the capture volume differed by a few orders of magnitude. Potentially more consequential are intermediate nitrogen-inversion rates in epimeric cases—since the energies of the interconverting species are unequal, a heavy bias against the eutomer might occur. The implications of an intermediate nitrogen-inversion rate are significant for in silico drug design, drug efficacy, molecular modeling of drug–protein binding, pharmacokinetics, drug enantiomer evaluation, etc. and thus due consideration of the process should be taken into account for drug development directions and *in vitro* evaluation.

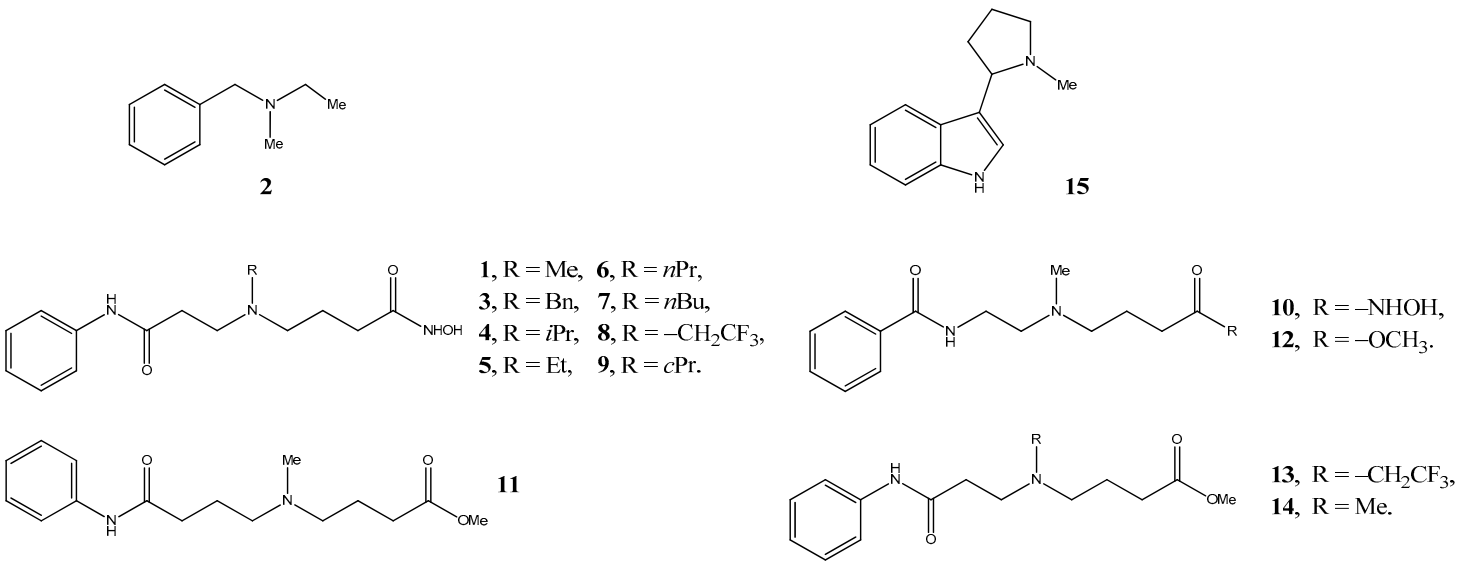

Figure S1. Structures of the compounds **1–15** examined in this work.

Table S1. Nitrogen-inversion rates and diffusion coefficients, *D*, for amines **1**–**15**.

Entry	Compound	Conc., mM	pH [a]	Solvent	Temp., °C	Inversion rate, s^{-1}	$D \times 10^{-10}$, m^2s^{-1}
1	**2·HCl**	19.8	HCl	CD_3OD	25	2.33, 0.25 [b] (T_c = 90 °C)	8.53
2	**2·HCl**	19.8	6	D_2O	25	–	5.12
3	**1·TFA**	64.4	8	D_2O	25	35.47	3.51
4	**1·TFA**	unknown	3	D_2O	25	3.60	3.51
5	**3·TFA**	unknown, sat. soln.	3	D_2O	25	6.86, 8.9 [b] (T_c = 45 °C)	3.20
6	**4·TFA**	25.7	3	D_2O	25	1.43	3.26
7	**14·HCl**	69.9	3.5	D_2O	25	1.24	3.81
8	**11**	156.2	4	D_2O	25	1.50	3.23
9	**14·HCl**	69.9	3.5	D_2O	37	5.32	5.40
10	**14·HCl**	69.9	6	D_2O	25	30–70 [b]	3.79
11	**10**	133.7	3	D_2O	25	5.46	3.45
12	**12**	107.8	3	D_2O	25	1.35	3.70
13	**10**	133.7	3	D_2O	37	13.96	4.91
14	**15·HCl**	20.0	7.5	D_2O	25	1.19	4.47
15	**5·TFA**	29.5	3	D_2O	25	45 °C [d]	3.41
16	**6·TFA**	31.2	3	D_2O	25	55 °C [d]	3.35
17	**7·TFA**	26.4	3	D_2O	25	55 °C [d]	3.23
18	**8**	unknown, sat. soln.	2.5	D_2O	25	magnetic inequivalence	–
19	**8**	unknown, sat. soln.	2.5	D_2O	37	magnetic inequivalence	5.09
20	**8**	unknown, sat. soln.	2.5	D_2O	100	reduced magnetic inequivalence	–
21	**8**	unknown, sat. soln.	2.5	D_2O	1.3	magnetic inequivalence + signal broadening	–
22	**9·TFA**	26.7	3	D_2O	25	45 °C [d]	3.36
23	**13**	~167	free base	$CDCl_3$	25	magnetic inequivalence	–
24	**13**	unknown, sat. soln.	2.5	D_2O	25	magnetic inequivalence	–
25	**13**	unknown, sat. soln.	2.5	D_2O	37	magnetic inequivalence	4.96
26	**13**	unknown, sat. soln.	2.5	D_2O	70	reduced magnetic inequivalence	–
27	**13·HCl**	unknown	HCl	DMSO	25	–	–
28	**13·HCl**	unknown	very low pH	DMSO	25	signals broad	–
29	**14·HCl**	69.9	7	PBS	25	–	–

[a] Or if the salt/free base was used. [b] The activation energy barrier, $\Delta G^{\ddagger}$, was calculated using the equation $\Delta G^{\ddagger} = 4.575 \times 10^{-3} \times T_c \times [9.972 + \log_{10}(T_c/\Delta\nu)]$ where T_c is the coalescence temperature and $\Delta\nu$ is the difference in Hz between the signals in the slow-exchange NMR regime. From $\Delta G^{\ddagger}$, the rate at 25 °C was calculated using the Eyring Equation. [c] Estimated. [d] A temperature indicates the change over from strong magnetic inquivalence effects to reduced effects.

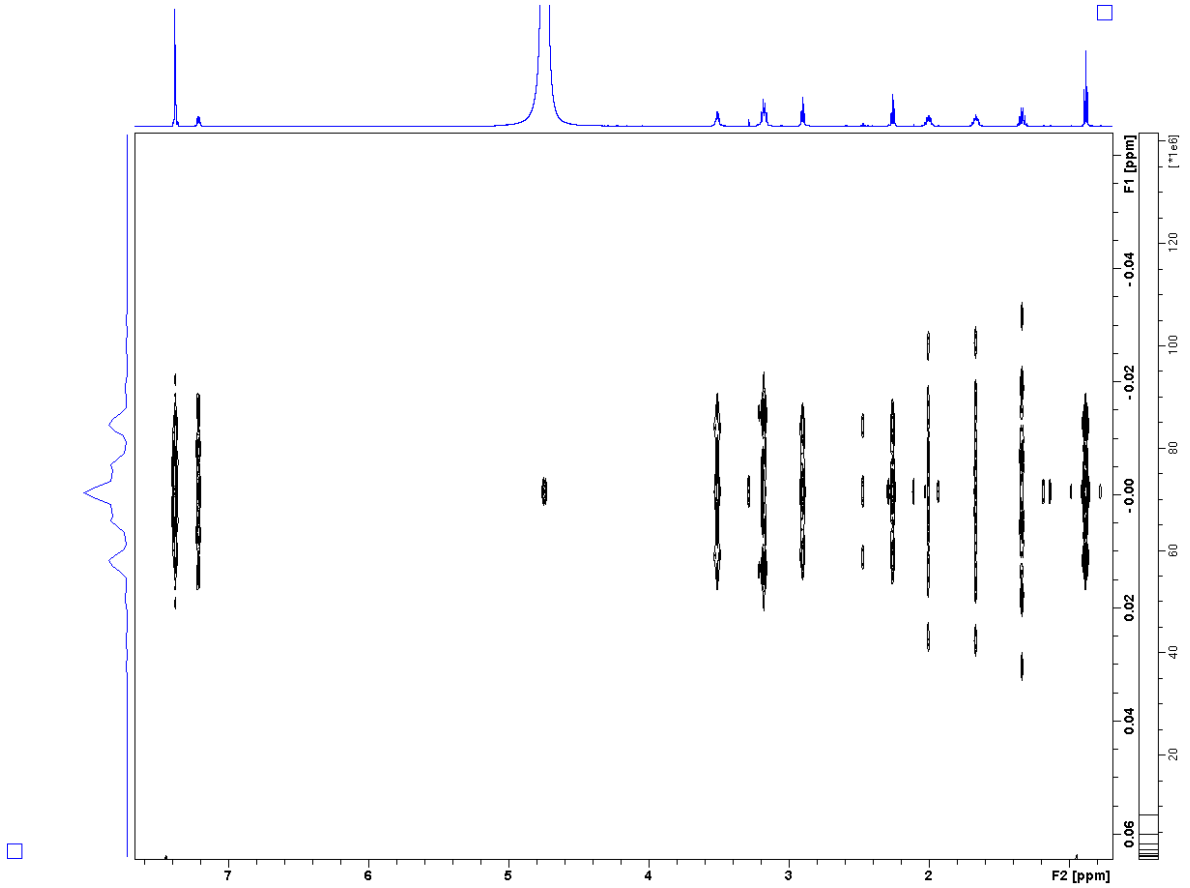

Figure S2. 2D *J*-resolved NMR spectrum of **7·TFA** in D_2O, pH 3 at 25 °C.

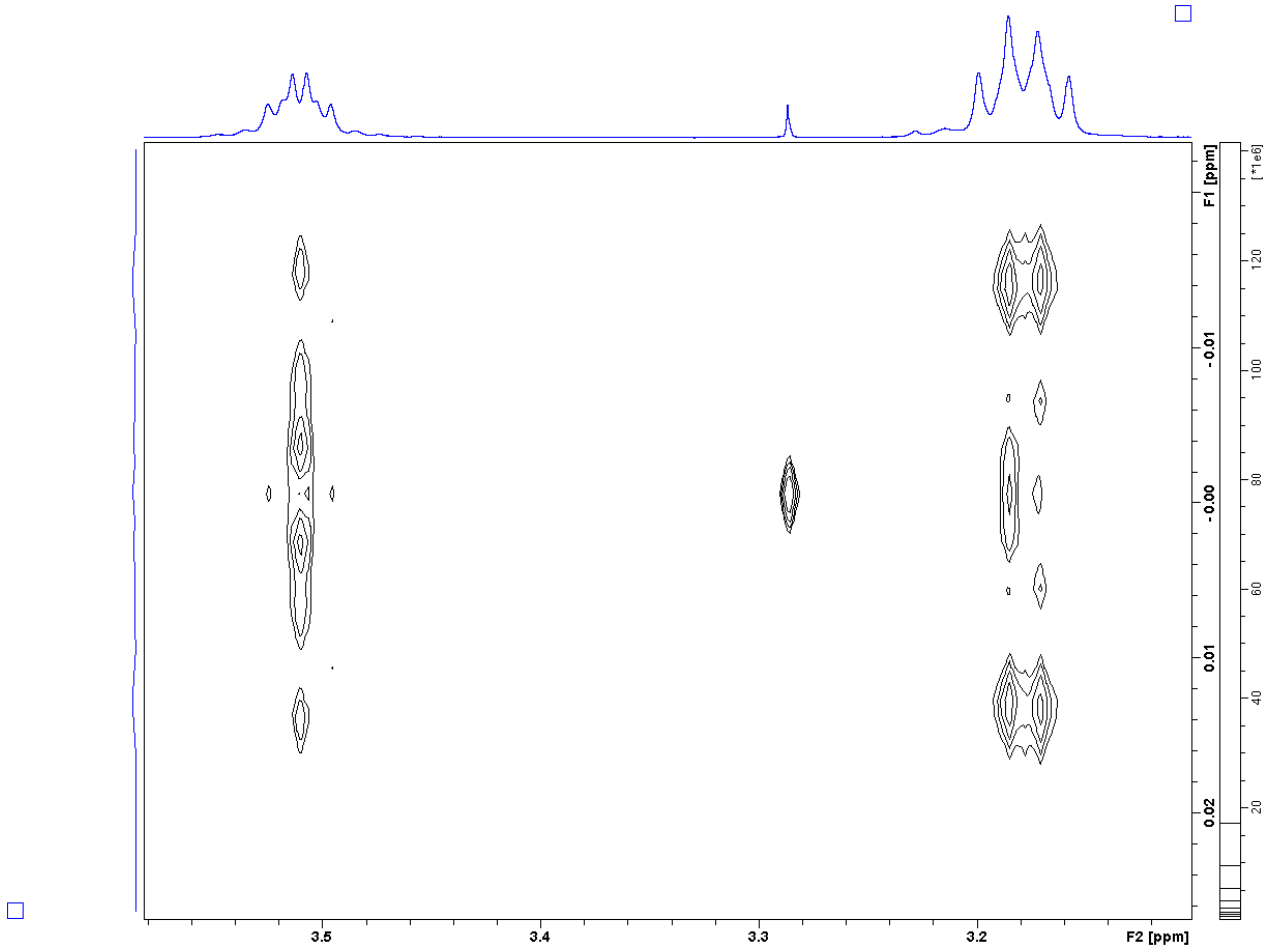

Figure S3. Expansion of the 2D *J*-resolved NMR spectrum of **7·TFA** in D_2O, pH 3 at 25 °C showing the α methylene of the ethylene segment (3.5 ppm) and the α methylene of the propylene segment (3.19 ppm) together with the α methylene of the butyl group (3.17 ppm).

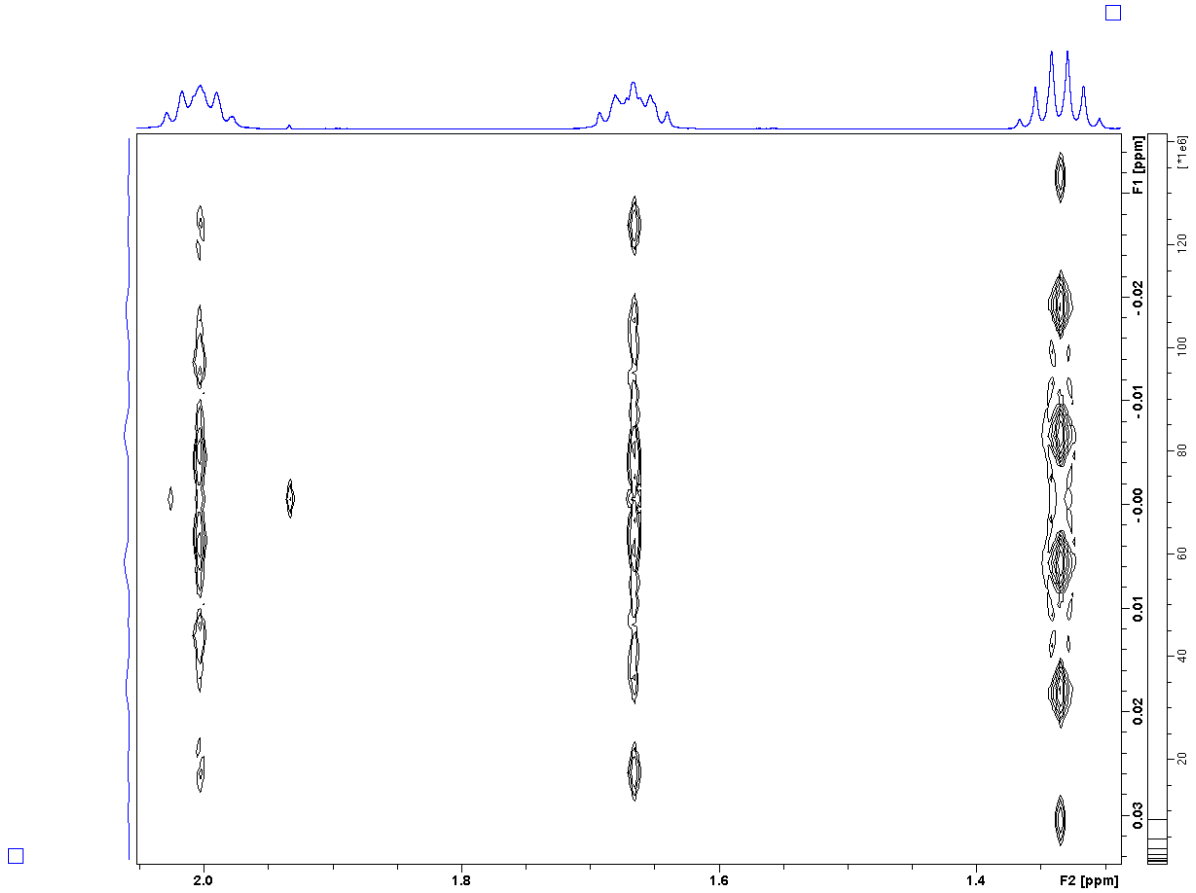

Figure S4. Expansion of the 2D *J*-resolved NMR spectrum of **7·TFA** in D_2O, pH 3 at 25 °C showing the β methylene of the propylene segment (2.0 ppm) and the β (1.7 ppm) and γ (1.3 ppm) methylenes of the butyl group.

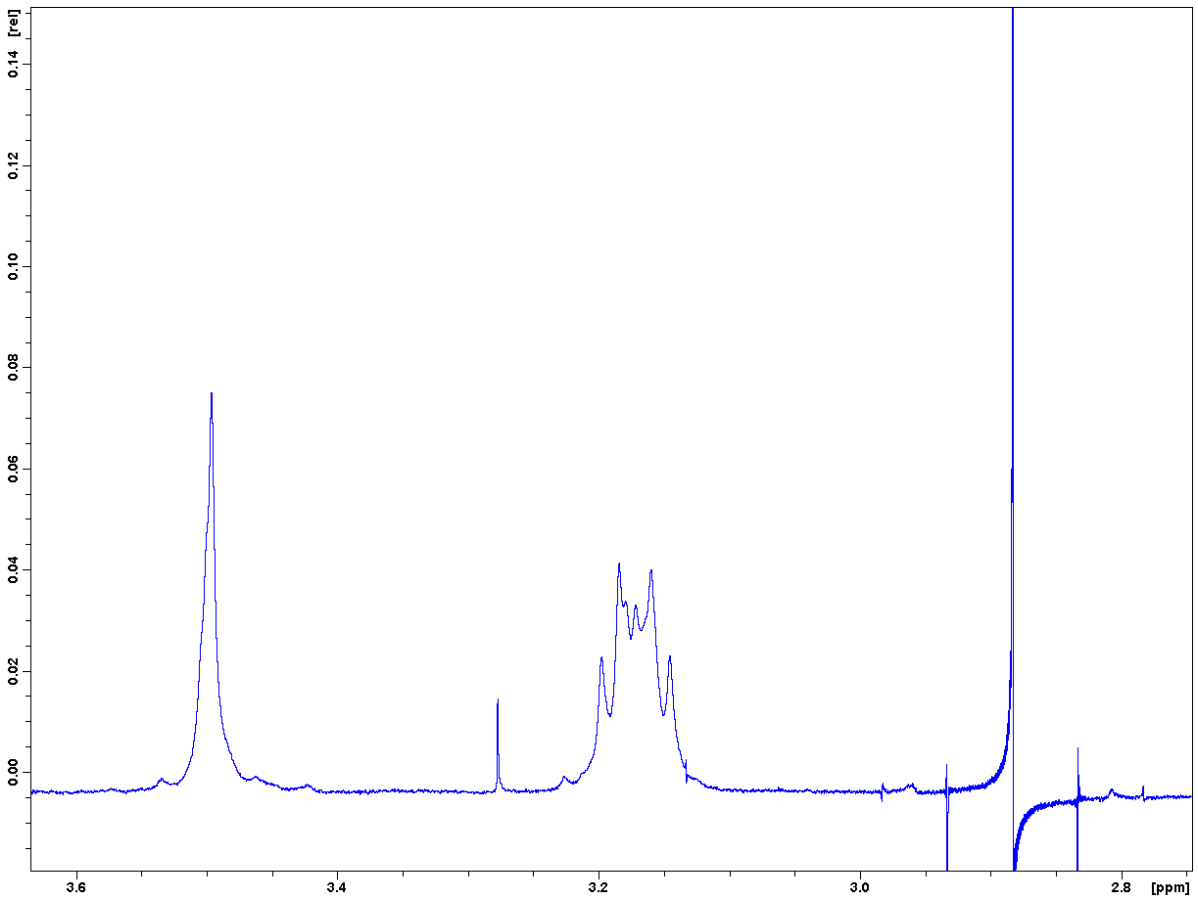

Figure S5. Homodecoupled ^1H NMR spectrum of **7·TFA** in D_2O, pH 3 at 25 °C with irradiation of the β methylene proton signal of the ethylene segment.

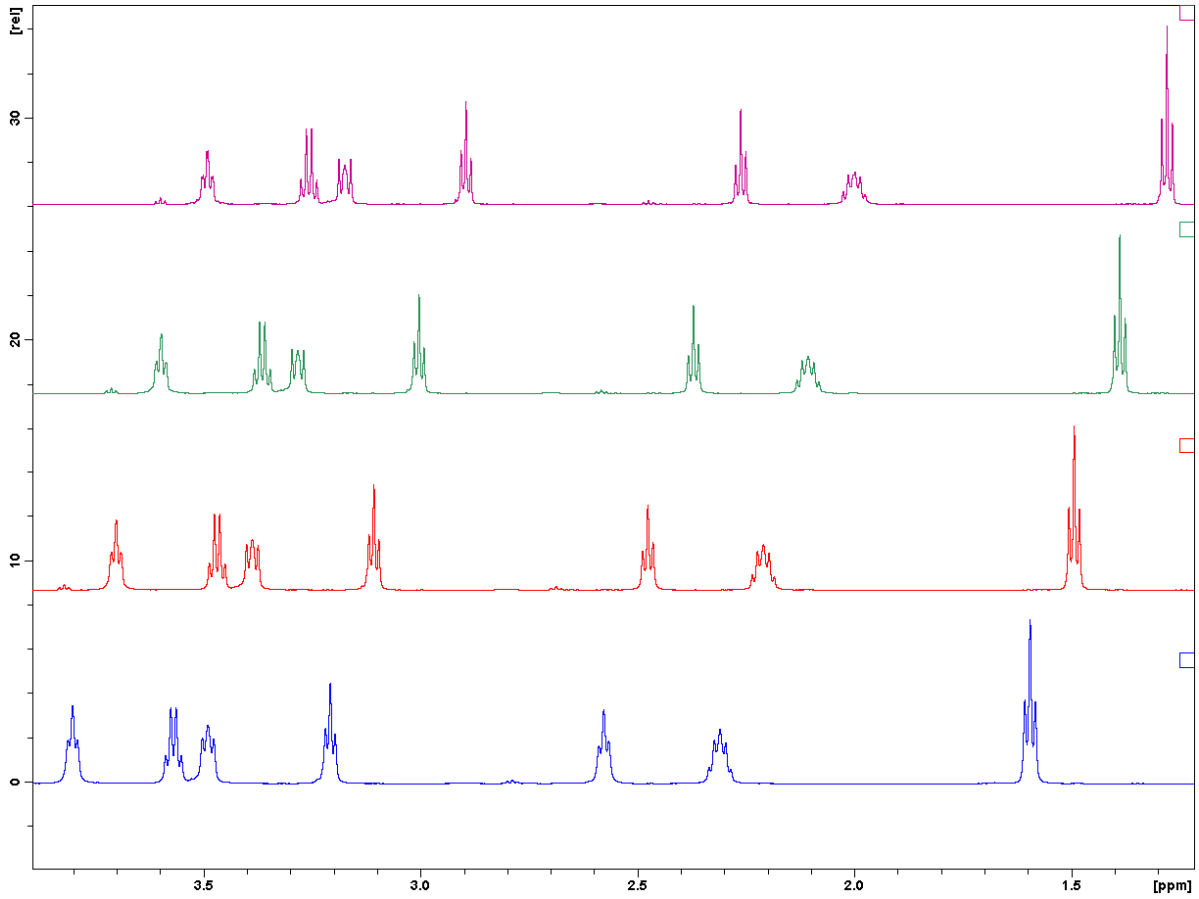

Figure S6. Alkyl region of the ^{1}H NMR spectra of **5·TFA** in D_2O, pH 3 at, from top to bottom, 25, 35, 45, and 55 °C.

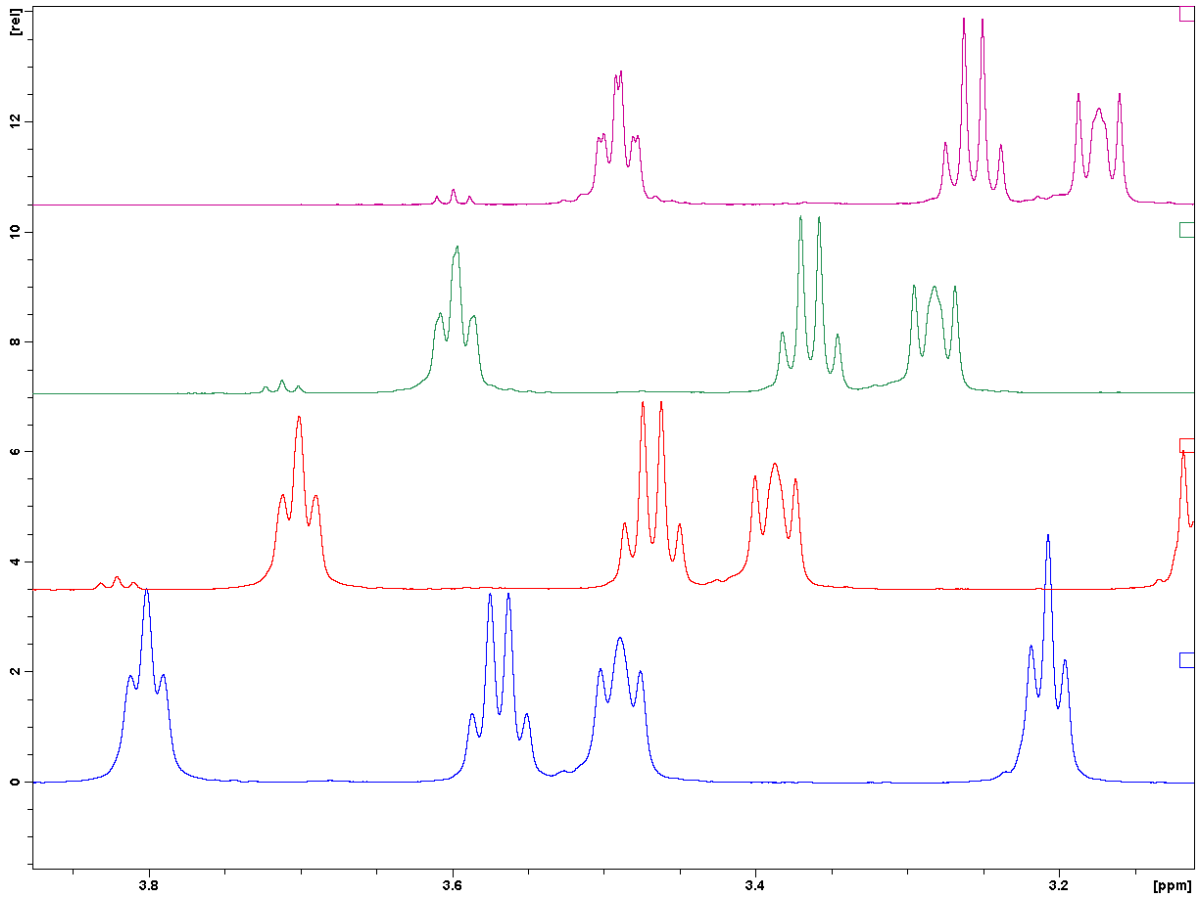

Figure S7. Expanded region showing the α methylenes and the β methylene of the ethylene segment of the ^{1}H NMR spectra of **5·TFA** in D_2O, pH 3 at, from top to bottom, 25, 35, 45, and 55 °C.

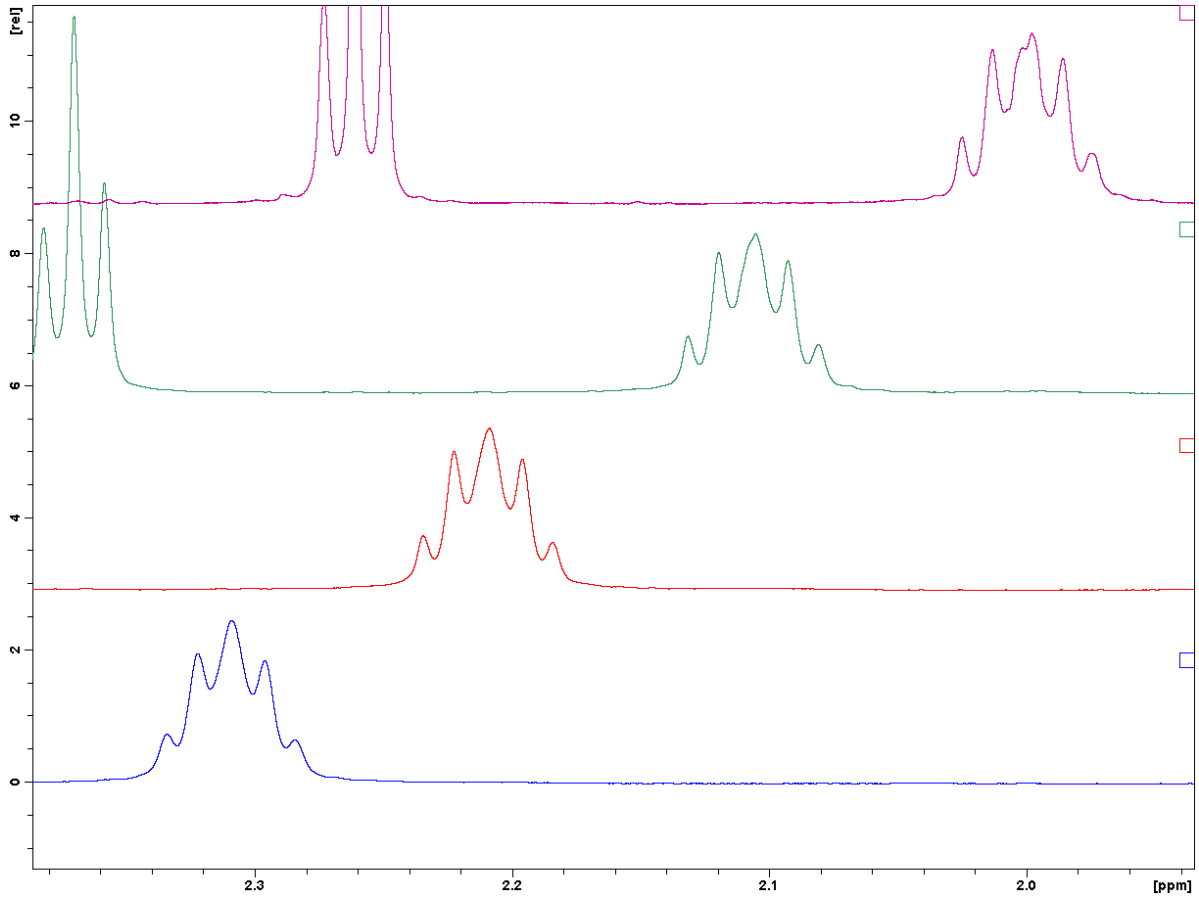

Figure S8. Expanded region showing the β methylene of the propylene segment of the ^{1}H NMR spectra of **5·TFA** in D_2O, pH 3 at, from top to bottom, 25, 35, 45, and 55 °C.

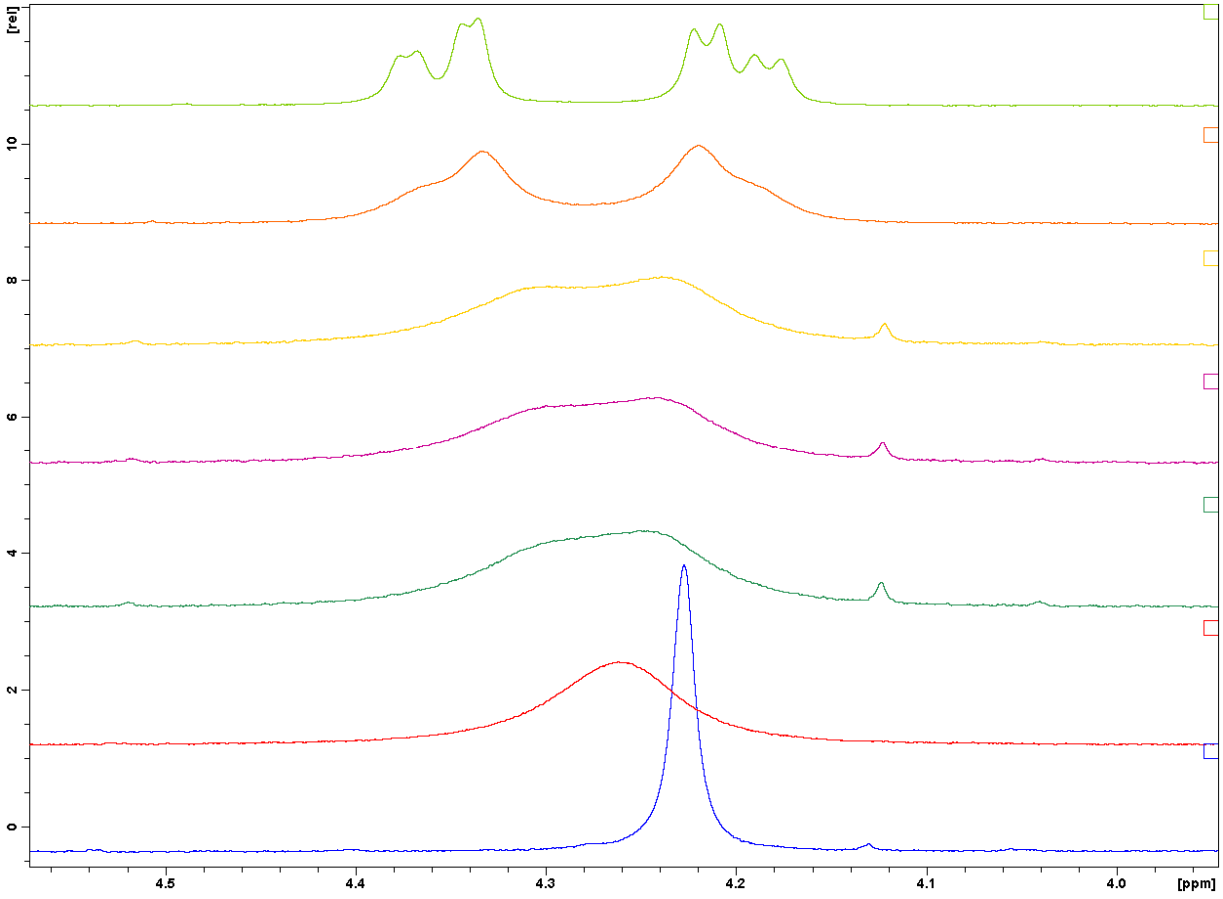

Figure S9. The methylene proton signals of the benzyl group in the ^{1}H NMR spectra of **2·HCl** in DMSO-d_6 at, from top to bottom, 25, 60, 80, 85, 90, 100, and 150 °C.